IEEE Robotics and Automation Letters (RAL) paper presented at
2024 IEEE/RSJ International Conference on Intelligent Robots and Systems (IROS)
October 14-18, 2024. Abu Dhabi, UAE

Transformable Inspection Robot Design and Implementation for Complex Pipeline Environment

Jianlin Wang, Yixiang Wang, Lining Peng, Haixiang Zhang, Hang Gao, Chengjiang Wang, Yuan Gao, Huanliang Luo, and Yongquan Chen, *Member, IEEE*

***Abstract*—Pipeline inspections are crucial to ensure the reliability of the transmission system. However, with the growing complexity and aging of the pipe system, traditional pipeline inspection robots struggle to adapt to complex environments with obstacles, cracks, changing cross-section, and other challenges. This letter introduces a novel transformable inspection robot with remarkable adaptability to varying pipeline environment from 163 mm to 312 mm inner diameter. The robot is composed of several motion modules that are arranged along its central axes at a 60-degree angle. The pneumatically powered robot has good active and passive deformation capabilities, enabling it to passively adapt to its surroundings and actively change between different postures. Our robot can also achieve automatic navigation in complex pipeline environments based on a LiDAR camera. Experiments demonstrate the robot adjusting to varying pipeline scenarios, including obstacles, diameter changes, turning up to 90 degrees, climbing up to 45 degrees, and crossing-section changes with a deformation rate up to 191.4%, overcoming the limitations of traditional designs.**

***Index Terms*—Pipeline inspetion robot, adapative robot, deformation robot.**

I. Introduction

PIPELINES have emerged as a solution to liquid resources transportation, especially for long-distance, considering their efficiency, cost-effectiveness, and minimal land use [1]. As reliance on pipeline systems intensifies, aging infrastructure suffers from many problems, including breakages, corrosion, and blockages [2]. Thus, prompt and effective inspection stands out as a pivotal aspect of pipeline management. The subterranean nature and remote locations of these systems, coupled with dark, confined, and hazardous environments, pose significant challenges for manual inspection [3].

To mitigate the risks of human inspection, pipeline inspection robots have been developed to address the aforementioned concern. Presently, pipeline inspection robots can be classified into three categories based on their locomotion mechanism, including wheeled, tracked and bio-inspired robots. Wheeled robots are extensively employed for inspection tasks within smooth, even, and predominantly straight short-distance transportation pipelines. Numerous studies including omni-directional [4], multi-linked configurations combined [5], adjustable-angle joints [6], wall-pressed [7], and screw-driven type [8], [9] have been conducted for greater flexibility and adaptability. However, wheeled robot still faces substantial challenges related to traverse irregular pipeline deformation, large obstacles and cracks. Tracked robots are another type to deal with rugged and uneven pipeline environments. To better adapt to varying pipeline conditions, independently adjustable modules [10], underactuated crawler modules [11], passive components on motion modules [12], and spherical omni-directional track design [13] have been introduced. Despite these innovations, tracked robot have inherent limitations including large size and lack of flexibility which resulting in reduced traversal capability when confronted within confined space and cracks. Bio-inspired pipeline inspection robot designs including snake-like with multi-degree-of-freedom joints [14] and inchworm-like robots including pneumatic soft robots [15] attracts considerable attention recently. Snake-like robots employ various propulsion methods, such as helical friction [16] and leveraging waveform oscillations [17]. Inchworm-like robots are normally driven by friction against pipe [18], linear contraction of front and back segments anchoring the pipe [19], [20], and tensegrity structure [21], [22]. Although they can move through very small pipes, their obstacle avoidance and crack traversal abilities are generally weaker, making them vulnerable to getting trapped in cracks.

Nevertheless, the majority of these robots are built to work in idealized pipelines that are straight, uniform, and unobstructed. In practice, pipelines often contain significant, such as limescale buildup from the deposition of calcium carbonate, cracks caused by external forces, and huge cross-sectional changes. Currently, no pipe robot is capable of overcoming such a multi-barrier environment that includes extensive longitudinal cracking, internal blockages, and changing cross-section. To solve the problems, we propose a novel pipeline inspection robot with large-scale active deformation and passive deformation abilities and it is

This work was supported in part by the Shenzhen Science and Technology Program under Grant JCYJ20210324115604012, Grant ZDSYS20220606100601002, and Grant KJZD20230923114810022, in part by the Science and Technology Program from General Administration of Customs of the People's Republic of China under Grant 2023HK072, in part by the Guangdong Basic and Applied Basic Research Foundation under Grant 2023A1515011347, in part by the Maxvision-AIRS-CUHK(SZ) Joint Laboratory of Inspection Robots, in part by Longgang District Shenzhen's "Ten Acion Plan" for supporting innovation projects under Grant LGKCSDPT2024002, and in part by the Shenzhen Institute of Artificial Intelligence and Robotics for Society.*(Corresponding author: Yongquan Chen.)*

Jianlin Wang, Yixiang Wang, Lining Peng, Haixiang Zhang, Hang Gao, Chengjiang Wang, Yuan Gao, and Yongquan Chen are with the Shenzhen Insti-tute of Artificial Intelligence and Robotics for Society, The Chinese University of Hong Kong, Shenzhen 518172, China (e-mail: yqchen@cuhk.edu.cn).

Huanliang Luo is with the Dapeng Customs of the People's Republic of China, Shenzhen 518083, China.

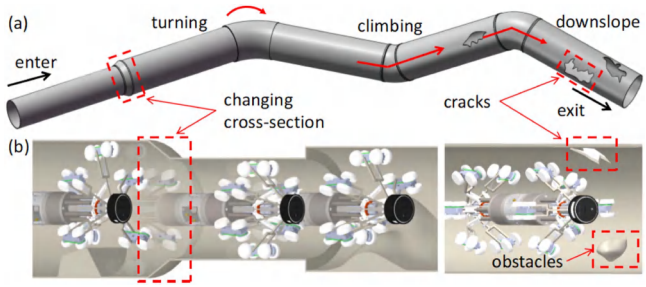

Fig. 1. Movement of the proposed transformable inspection robot in a complex pipe environment. (a) Complex pipeline environment with changing cross-section, turning, climbing, obstacles, and cracks. (b) Diagram of the robot moving in the above scenario.

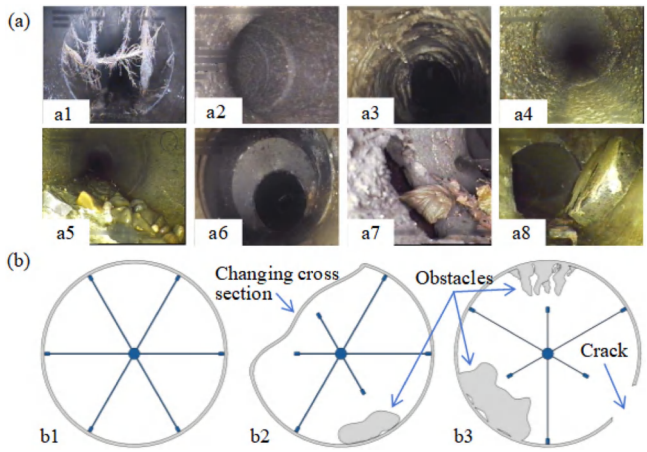

Fig. 2. Robot design idea. (a) The pictures of real pipeline environments in different scenarios. (b) Schematic depiction of the robot in a complicated environment is shown in sectional view.

expected to adapt to complex pipeline environment as illustrated in Fig. 1. The robot can navigate through complex and varied pipeline environments with high adaptability. And the contributions of the letter are listed as follows:

- We present a novel transformable pneumatic powered robot with active and passive adaptation mechanisms. The robot is able to constitute to different postures with a deformation rate up to 191.4%.
- We propose a pneumatic robot control system with online vision-servo feedback to realize automatic navigation in linear complex pipeline environment, and this system facilitates both manual and automatic operation.
- Ground experiments in complex environments are carried out to verify the robot's advanced motion capabilities, including navigation through irregular pipe breakages, variable cross-sections like diameter and shape alterations, and obstacles such as stones, tree branches and incrustation.

This letter is organized as follows. Sections II, III, and IV introduce the idea, mechanical, and control system. Sections V and VI present the experiments and conclusions.

II. Robot Design Idea

To address the issues that pipeline inspection robot field is now confronting, we firstly analyze the cross-sectional view of the real pipeline as described in Fig. 2(a) including numerous obstacles, changing cross-sections, cracks, turnings, and climbing [23]. Due to the complex layout of the actual pipeline's interior environment, with unpredictable obstacles and cracks of varying forms. Designing a robot with the capacity to overcome all obstacles and cracks would be a formidable undertaking, and it would heighten the probability of the robot becoming trapped. Hence, it is more advisable to avoid rather than overcome those hurdles and cracks. Besides, there are also some tiny gravel particles and uneven ground in the pipeline environment as shown in Fig. 2(a3) and (a4). Although the robot may have challenges when maneuvering past large impediments and fissures, it is capable of successfully overcoming small obstacles and uneven terrain by employing its motion module. Consequently, this implies that the robot can utilize a multitude of motion modules in order to offer assistance and drive itself forward while aiming at small obstacles and uneven terrain.

Therefore, the robot design would follow two principles: active deformation to avoid big obstacles and cracks that cannot overcome by motion modules, and passive deformation to overcome small obstacles and uneven ground which is less likely to stuck the robot. Incorporating more motion modules can optimize the range of flexible poses that the robot can achieve by counterbalancing the force of gravity. Simultaneously, an excessive number of motion modules will elevate the minimum limit of the robot's motion range to a level that prevents it from traversing through small pipes. Hence, we decided on an amount of 6 motion modules. As shown in Fig. 2(b1)–(b3), the six self-symmetric motion modules are intended to supply enough power and improve stability. The robot could also have multiple postures by stretching or constricting the modules actively with a large deformation rate. For the passive deformation, a redundant degree of freedom is given at the motion modules, and pneumatic-driven is used. Both can provide better interaction with the environment and allow the robot to have continuous contact with the surroundings. As illustrated in Fig. 1, the robot is expected to navigate in a complicated pipeline environment by active and passive deformation.

III. Mechanical System Design

Based on the robot design ideas concluded, the mechanical system architecture of the robot with morphing abilities in both active and passive states is shown in Fig. 3. The robot is characterized by a symmetrical structure with multiple motion modules distributed evenly along its center line to increase the agility and stability of the robot. It is composed by three modules: the propulsion module to implement the posture adjustment of the robot, the central module to constitute the skeleton of the robot, and the motion module to realize the motion ability of the robot.

A. Propulsion Module

As stated in Fig. 3(a), the propulsion module consists of the front cover, body, bottom cover, joints and push rod. Different

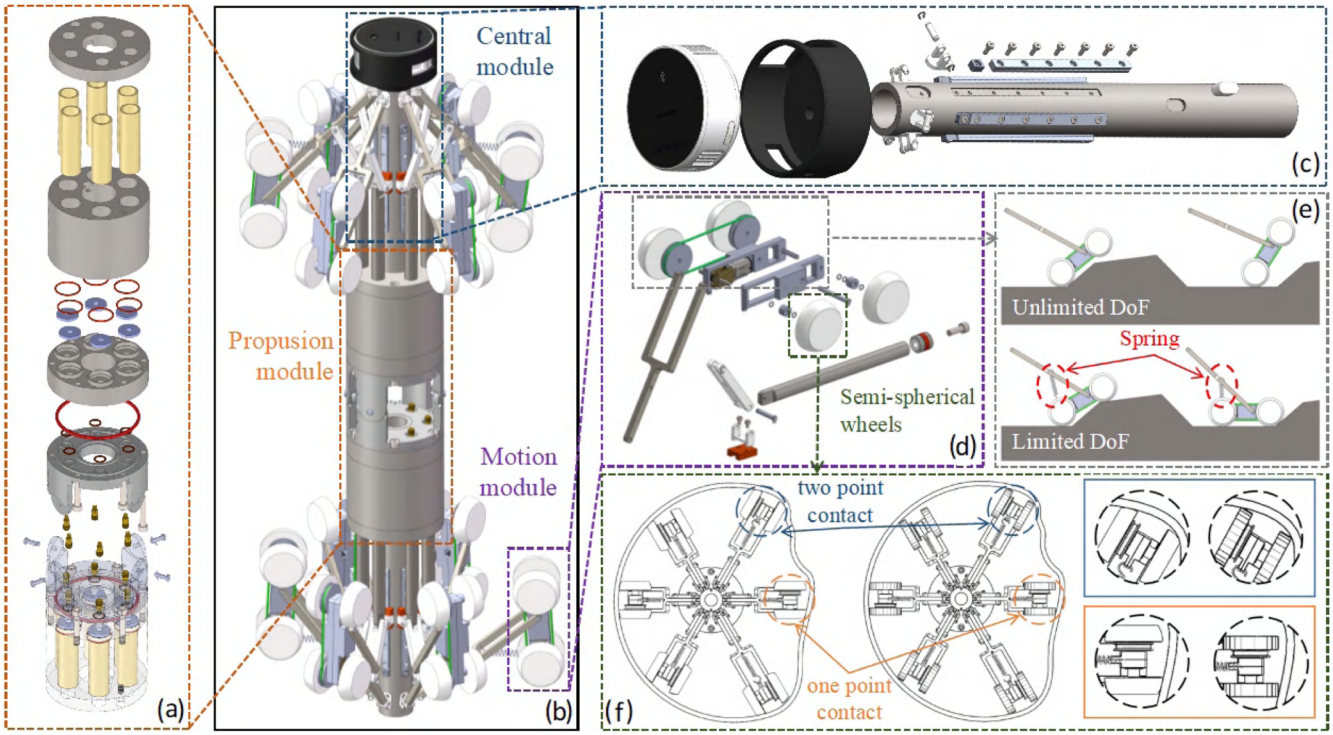

Fig. 3. Mechanical system architecture of our robot. (a) Explosion view of the propulsion module. (b) CAD of the prototype robot. (c) Explosion view of the central module. (d) Explosion view of the motion module. (e) Comparison of movement of the motion modules between with and without limitation provided by spring. (f) Comparison of the interaction with cross-section pipeline environment between the semispherical wheels and regular wheels.

sizes of rubber seal rings and gaskets are installed to ensure air tightness, which improves the stability and work efficiency of the equipment. Brass bushings are incorporated in each chamber to reduce friction and wear on the components. The movement of the module relies on air pressure supplied by a pump and delivered via tubing to the air pipe joint, which drives the piston to go forward or backward in response to the changes in air pressure in the chamber. The piston is equipped with V-shaped seal rings to ensure the airtight integrity of the chamber and slides along the wear-resistant brass bushing as the air pressure changes. The pneumatic nature of the drive allows the robot to passively deform with external forces, enabling it to overcome some small, unforeseen obstacles effortlessly.

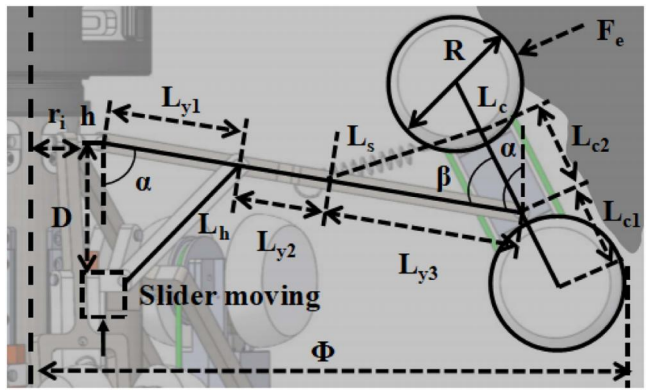

Fig. 4. Schematic diagram of working space analysis with key parameters.

B. Motion Module

The motion module, depicted in Fig. 3(d) is affixed to the central module and can adjust the robot's posture. The motion modules also provide multiple contact points with the environment, thus ensuring robust locomotion in the pipe by delivering ample power. Furthermore, to enhance terrain adaptability, a redundant degree of freedom is added. As illustrated in Fig. 3(e), the design improves the robot's ability to adjust its posture, resulting in increased versatility. A spring is included to limit the range of motion and prevent structural misalignment that may impede movement. It allows the robot to have multiple potential configurations, optimizing its effectiveness in various conditions. In a departure from traditional round wheels, the robot employs semispherical rubber wheels as implemented in Fig. 3(f). The two scenarios in the figure demonstrate that the semispherical rubber wheel performs better and has a bigger contact area with not only common curved surfaces but also specific cross-sections. The elasticity of rubber also allows the wheels to deform slightly, conforming to the surface for a better grip.

C. Working Space Analysis

The working space Φ of the robot, as shown in Fig. 4, depends on two revolution degrees of freedoms, α and β, one depends on the active movement of the slider, and another one is passively impacted by the environment it interacts with. As the air pump's input and output states change, the slider swings forward and

backward until it eventually finds equilibrium with the outside force F to create a certain angle α. In addition, a certain angle β is produced passively by the spring and outside forces. By assuming the spring constant is k and the friction is small enough to ignore. Other key parameters that influence the working space of the robot are the relative distance between the slider and the retaining bracket D, the length of Y-shaped and H-shaped connecting rod L_h (44 mm) and L_y (115 mm), length of motor case L_c (62 mm), the distance between central line of the robot and connecting rod fastener r_i (13 mm), height of fasteners h (6 mm), diameter of semi-spherical wheels R (36 mm) and the initial length of spring is L_{s0}. We are able to define the angles as:

$$L_h^2 = L_{y1}^2 + D^2 - 2L_{y1}D\cos\alpha \tag{1}$$

$$\alpha = \arccos\frac{L_{y1}^2 + D^2 - L_h^2}{-2L_{y1}D} \tag{2}$$

$$\left(\sqrt{L_{y3}^2 + L_{c2}^2 - 2L_{y3}L_{c2}\cos\beta} - L_{s0}\right) \times k = F_S \tag{3}$$

$$F_S \times L_{c2} = F_e \times (L_c - L_{c1}) \tag{4}$$

$$\beta = \arccos\frac{(\frac{F_e(L_c-L_{c1})}{L_{c2}k} + L_{s0})^2 - L_{y3}^2 - L_{c2}^2}{-2L_{y3}L_{c2}} \tag{5}$$

Based on the value of the two angles calculated, the working space can be described as follows. Besides, they are limited to boundaries: $\alpha \in [15°, [81°]$, $\beta \in [30°, [103°]$.

$$\Phi = r_i + h + L\sin\alpha + (L_c - L_{c1})\sin(\alpha - \beta) \tag{6}$$

D. Turning and Climbing Analysis

The turning and climbing capacity of pipeline inspection robots has also drawn a lot of attention. For our robot, its turning and climbing ability is demonstrated in Fig. 5(a) and 5(b) respectively. According to the formal below, we are able to calculate the minimal turning radius of the robot under limited conditions with inner diameter R_i, outer diameter pipeline R_o, total length of the robot L (568 mm), the width of the central module as d and turning angle as θ_i:

$$R_o^2 = \left(R_i + \frac{d}{2}\right)^2 + \left(\frac{L}{2}\right)^2 \tag{7}$$

Besides, the inner diameter of the pipe $D_p = (R_o - R_i)$ should be bigger than the minimum working space:

$$R_i = \frac{L^2}{8(D_p - \frac{d}{2})} - \frac{2D-d}{4}, (R_o - R_i) \geq \Phi_{\min} \tag{8}$$

Simultaneously, depending on the robot's deformable properties, the power in a complex environment may come from a limited number of motion modules by interacting with the surroundings. As shown in Fig. 2(b2) and (b3), it can endure gravity with a maximum of two motion modules. Assume there are n_f and n_b motion modules used to endure the gravity of the robot in the front and back parts respectively. The number of other motion modules in the stretch state is m_f and m_b, and the totally number of all stretched motion modules is N_s.

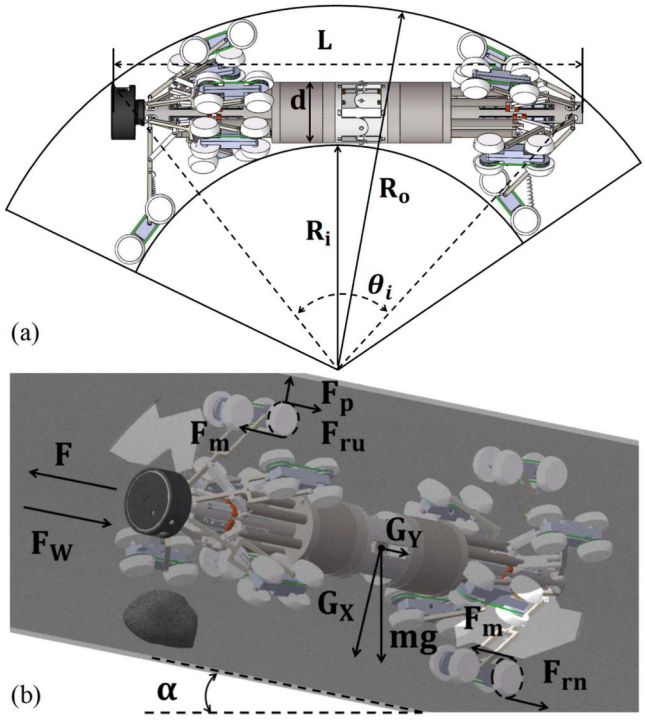

Fig. 5. Robot motion ability analysis. (a) Schematic diagram of robot in a turning pipeline. (b) Schematic diagram of robot in an inclined pipeline.

The number of stretched motion modules is limited: n_f and $n_b \in [1, 2]$, m_f and $m_b \in [0, 4]$. Assume the driving force of a single motor is F_m, the total driving force F of the robot is:

$$N_s = n_f + n_b + m_f + m_b, F = \sum_{i=0}^{N_s} F_m \tag{9}$$

For the robot with gravity $G = mg$ is climbing on a slope with an angle of inclination as θ, assume the friction coefficient as μ, and the tire and the ground adhere sufficiently with no slide, and the resistance created is rolling resistance as F_{rn} for nether motion modules with gravity applied. For others, the force F_p caused by air pressure from the chamber influences the rolling resistance F_{ru}. Assume the acceleration resistance is F_W, we can get the rolling resistance as:

$$F_{rn} = \mu(mg\cos\theta + F_p), F_{ru} = \mu F_p \tag{10}$$

$$F = \sum_{i=0}^{n_f+n_b} F_{rn} + \sum_{i=0}^{m_f+m_b} F_{ru} + mg\sin\theta + F_W \tag{11}$$

Disregard the effects of acceleration resistance F_W when the speed is low:

$$\sum_{i=0}^{n_f+n_b+m_f+m_b} F_m = \sum_{i=0}^{n_f+n_b} (\mu(mg\cos\theta + F_p)) + \sum_{i=0}^{m_f+m_b} (\mu F_p) + mg\sin\theta + F_W \tag{12}$$

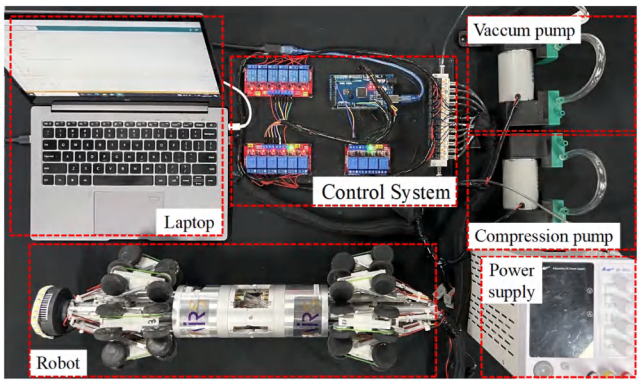

Fig. 6. Hardware system of the prototype robot.

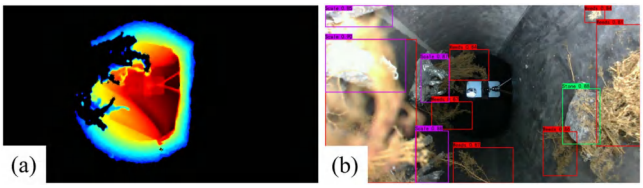

Fig. 7. Environment perception based on L515 lidar camera for complex pipe. (a) Depth images of internal pipeline with obstacles. (b) Multi-label images of objects may appear inside the pipeline.

IV. Control System Design

A. Hardware Subsystem

The comprehensive layout of the robot system is shown in Fig. 6, it uses a laptop for high-level control which can interact with a low-level controller and actuators. Additionally, the system integrates pumps, power supply, and the prototype of the robot. The hardware of the system comprises a microcontroller (Arduino Mega 2560 R3), relays, pneumatic solenoid valves, a 12-position 3-way manifold, compression and vacuum pumps (UV-U3, 12 V, 24 W), and a power supply. As illustrated in the previous figure, 12 solenoid valves (OST Solenoid SY3/2NC, 12 V, 1 W) and the manifold serve as intermediaries, bridging the individual chambers with the compression and vacuum pumps. The microcontroller dispatches signals to two 6-way relays, thereby regulating the solenoid valves' operations and ensuring the independent control of each air chamber. The low-level controller can receive commands from either a high-level controller or manual input. It can further change the state of solenoid valves to make the targeted motion modules extend or contract respectively to help the robot adapt to complex environments autonomously.

B. Vision Subsystem

The potential of auto-driving has been explored to reduce the reliance on human operators based on the vision subsystem. A LiDAR camera L515 with an Inertial Measurement Unit (IMU) inside has been equipped on the central module to perceive the environment. As shown in Fig. 7, we have collected a new RGB-D dataset of simulated pipeline interiors using the robot, including depth images and multi-label images, as shown in Fig. 7(a), and (b) respectively. The dataset is collected with a resolution of 640*480 pixels of about 5000 pairs of RGB and depth images from videos. It is annotated with common obstacles including stones, silt, weeds, and cracks. Several object detection algorithms are tested based on our dataset to equip the robot with autonomous obstacle avoidance capabilities. The performance of these detectors, as summarized in Table I, was assessed based on average precision (AP) and frames per second (FPS) processed during inference. According to the test, YOLOv8 outperformed the others regarding accuracy and processing speed. Therefore, we have utilized YOLOv8 in the Laptop to complete real-time obstacle identification in sophisticated pipeline environments.

TABLE I
Performance Comparison of Various Object Detectors on Our Pipeline Datasets With Same Input

Model	Year	Backbone	AP 0.5	FPS
SSD	2016	Vgg16	89.91%	77.4
RetinaNet	2018	ResNet-101-FPN	89.13%	26.04
YOLOv3	2018	DarkNet53	78.57%	18.03
YOLOv8	2023	YOLOv8_x	96.59%	33.79

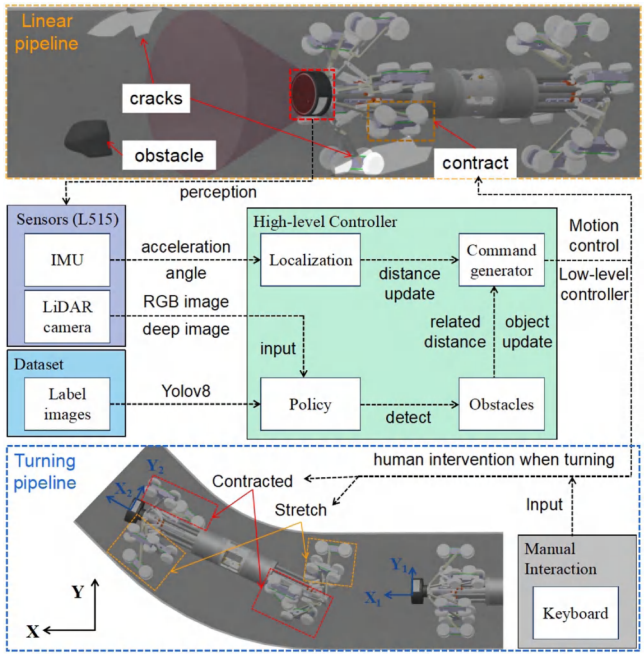

Fig. 8. Operation workflow of the robot in the linear and turning pipeline: The robot perceives obstacles and cracks in the pipeline and takes action based on commands given by a high-level controller automatically; motion can also be manually intervened under special scenarios like turning.

C. Motion Control Subsystem

The operational workflow of the robot system is illustrated in Fig. 8. The information including RGB images, deep image, and data from IMU, is transmitted to the high-level controller, which is the Laptop in the system. Obstacles would be detected based on the policy and the relative distance between the robot and

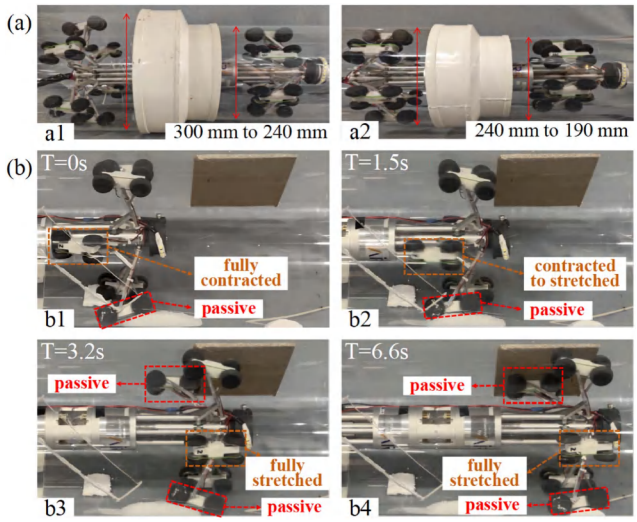

Fig. 9. Prototype of the transformable adaptive pipeline inspection robot. (a) The prototype goes through a changing inner diameter pipeline with good deformation ability. (b) The prototype adapts to the pipeline with active and passive deformation.

obstacles would be recorded as D_o at time t_m. When obstacles fall outside the robot's detection range, the relative distance between the robot and each obstacle would be updated based on the IMU data. The safe distance for the robot to take action is D_s, the velocity at time t_m is V_m, and the traveling distance for the robot at time t_m is D_m. The equations are shown below:

$$D_{m+n} = D_m + \sum_{t=m}^{m+n} (V_m + a_t) \tag{13}$$

$$\begin{cases} taking \quad actions, & D_s > D_o - (D_{m+n} - D_m) \\ no \quad actions, & D_s \leq D_o - (D_{m+n} - D_m) \end{cases} \tag{14}$$

The high-level controller would generate corresponding commands to the low-level controller when the distance between the robot and obstacles is smaller than D_s. In addition to the automatic control based on vision, the robot can also be controlled manually under some special scenarios like turning as shown in Fig. 8. The motion modules of the front part of the robot with the inner circle and the back end with the outer circle will contract, and others stretch to change the posture of the robot to pass through the turning.

V. Experiments

A. Prototype Test

A prototype of the transformable adaptive pipeline inspection robot is manufactured and assembled as shown in Fig. 9. The robot is capable of executing movement within pipelines of varying inner diameters as shown in Fig. 9(a), and it can navigate through complicated pipelines by utilizing active and passive deformation in Fig. 9(b). The changing posture of the transformable robot could influence the number of motion modules in contact with the surroundings and it would significantly affect the power and motion speed of the robot. Another factor that significantly influences the velocity of the robot would be the slope. In Fig. 10(a) shows the robot moves in different postures with one to six motion modules applied respectively, Fig. 10(b) indicates that the robot is ascending slopes with angles of 15, 30, and 45 degrees correspondingly and Fig. 10(c) shows the robot doing turning with 30, 60 and 90 degrees. Fig. 10(d) and (e) depict the average velocity of various postures and slopes with mean value and median value. It indicates the maximal speed of the robot could be 23.8 millimeters per second derived from 10 individual test outcomes for each situation and could be 2.3 times quicker than moving with only one motion module, and despite being able to ascend 45-degree slopes, the robot finds it extremely challenging. The attitude change of the robot related to time during turning is shown in Fig. 10(f) and it shows the robot is able to turn up to 90 degrees in a pipeline with an inner diameter of 315 millimeters.

B. Experiment Test

To validate the experiment's authenticity, a test environment, designed to imitate real-world circumstances, is established with a length of 5 meters, as seen in Fig. 1(a). Based on that, the experiments are performed to demonstrate the performance of the transformable inspection robot. The comprehensive adaptability to complex environments of the robot has been fully demonstrated as described in Fig. 11. The Fig. 11(a), 11(b), 11(c), and 11(d), examined the robot's adaptability to changing cross-sections, turning, obstacles and slope, respectively. Obstacles and fissures are commonly incorporated into most settings to accurately recreate the real surroundings to the finest detail possible.

C. Result and Discussion

The proposed robot shows good performance for the complex pipeline environment with various postures. The weight of the assembled robot is 3.86 Kg, and the total length of the robot is 568 mm. The comparison of performance of the proposed robot is compared with the previous pipeline inspection robots as shown in Table II. Our robot illustrates a novel mode of locomotion that differs from existing robots, relying on both active and passive deformation. Our robot is capable of changing into various configurations in order to negotiate intricate pipeline conditions than others cannot. Our robot outstands in deformation rate, turning, and adapting to complex real pipeline environment with obstacles and cracks. Besides, our robot also demonstrates the ability to navigate automatically in a straight pipeline with sensing.

At the same time, our robot also revealed some areas worth improving. Firstly, lack of climbing ability. Our robot now cannot climb over 45 ° slope because of a weak power relative to its weight and it could be solved by using more powerful motors and reducing the weight of the robot. Secondly, no accuracy localization. The localization of a robot relies entirely on an Inertial Measurement Unit (IMU), which is prone to drift and susceptible to external environmental factors. Consequently, this might result in the robot's deformation being activated too early or too late, causing it to become stuck on cracks or impediments.

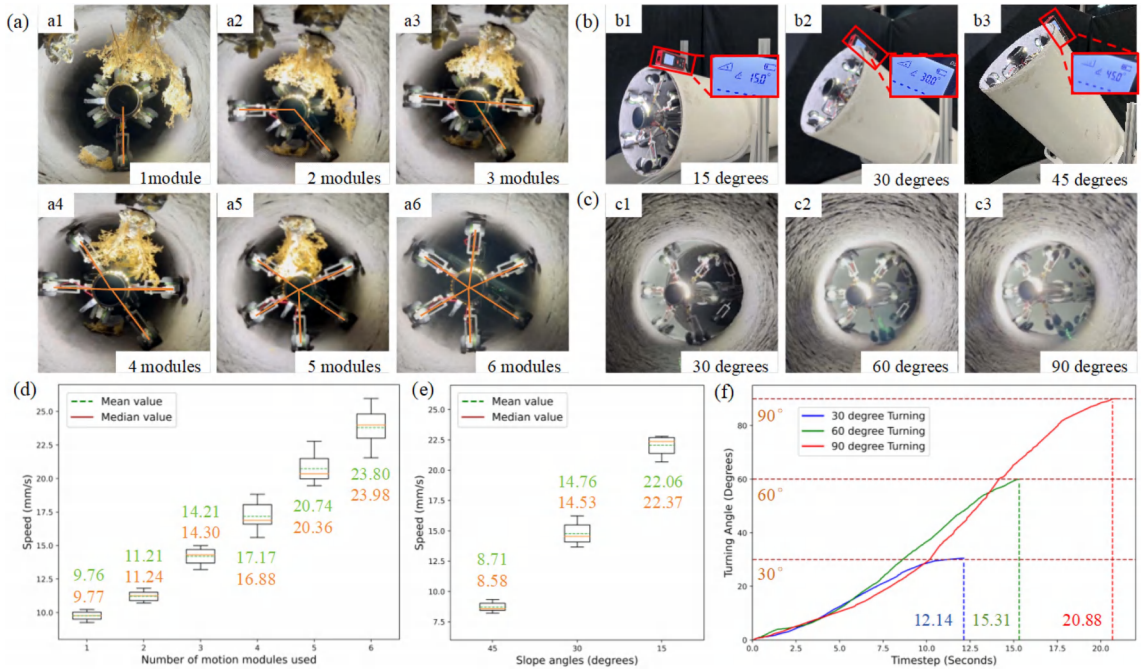

Fig. 10. Motion ability test for different postures and slopes. (a) Motion test of the robot in a straight pipe with different number of motion modules from 1 to 6. (b) Motion test of the robot on slopes with different angles including 15, 30 and 45 degrees. (c) Motion test of the robot with different turning angle including 30, 60 and 90 degrees. (d) The speed of the robot moving with different number of motion modules. (e) The speed of the robot with different slope angle. (f) Changing curve of turning angles related to time.

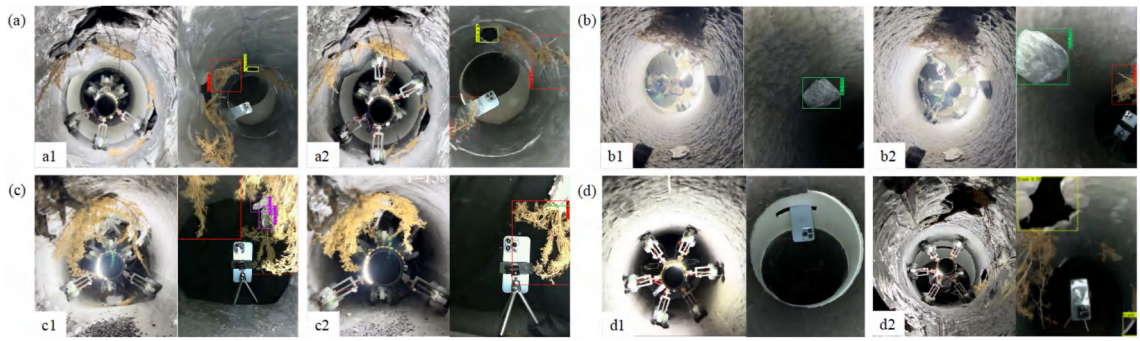

Fig. 11. Experiments of the robot for different scenarios. (a) Changing cross-sections pipeline with cracks. (b) Turning pipeline with obstacles. (c) Complex pipeline with obstacles and cracks. (d) Pipeline with slopes including both ascending and descending.

TABLE II
COMPARISON OF PREVIOUS PIPELINE INSPECTION ROBOTS AND OUR ROBOT

Robot	Working Space	Deformation Rate	Turning	Climbing	Obstacle	Crack	Auto-driving	Sensing
Edwin Dertien[4]	63-125 mm	201.6 %	90°	0°	✗	✗	✗	✗
Young-Sik Kwon[5]	80-100 mm	125 %	90°	0°	✗	✗	✗	✓
Hiroaki Fukushima[9]	150 mm	0%	90°	00°	✗	✗	✗	✗
Atsushi Kakogawa[11]	154-202 mm	131.2 %	0°	0°	✗	✗	✗	✗
Kartik Suryavanshi[13]	160 mm	0%	90°	90°	✗	✗	✗	✗
Mariko Inazawa[16]	194 mm	0%	90°	90°	✗	✗	✗	✗
Atsushi Kakogawa[14]	101-127 mm	125.7 %	90°	90°	✗	✗	✗	✗
Jiawei Cao[15]	102-122 mm	119.6 %	0°	≈ 30°	✗	✗	✗	✓
Yixiang Liu[21]	100-180 mm	180 %	45°	90°	✗	✗	✗	✗
Our robot	**163-312 mm**	**191.4** %	**90°**	**45°**	✓	✓	✓	✓

More sensors are considered for the next generation of robots. Thirdly, no highly integrated robot system. The robot still requires connections to external power supply, controls and others and the motion range may be limited to these extrinsic factors. Lastly, incomplete control system. Currently, the environment is seen solely through a LiDAR camera. However, this camera may have blind spots as it rotates, resulting in the failure to detect impediments and causing the robot to get trapped in certain situations. As a result, the robot now can only achieve automatic navigation in a linear pipeline. The automatic driving at turning in a pipe filled with obstacles and cracks remains a challenging task in a complicated environment. Besides, the judgment strategy applied now is only based on the category of obstacles without the consideration of obstacle sizes. Therefore, the approach of active deformation may be employed for impediments that are small enough to be overcome by passive deformation, it may prevent the robot from reaching the most effective moving capabilities.

VI. Conclusion

This letter introduces a robot design theory based on active and passive deformation adapting to the complex real pipeline environment and the prototype is designed and tested. The transformable adaptive pipeline inspection robot design can work in complex real environments, an area that has not been extensively explored previously. The robot is able to achieve multiple postures with a big deformation rate and good motion ability for turning and climbing which help the robot navigate through intricate surroundings with ease. The experiments demonstrate the robot's capacity to adjust to different pipeline conditions, utilizing both active and passive deformation capabilities. According to the control system, the robot is capable of autonomous navigation for linear pipelines. For future work, we will refine the prototype and build new pipeline robots by sticking to the following principles: multi-postures, big deformation rate, and active and passive deformation. The structure will be further developed for lighter weight and a bigger deformation rate. Besides, we will consider developing an integrated robot system with more perception sensors to realize comprehensive detection of the environment to achieve automatic driving at turning and more accurate identification of obstacles. Moreover, we are planning to expand the dataset with more types and number of obstacles by working together with industry partners and improving detection and identification of turning in intricate scenarios for full autonomous navigation in real pipelines.

References

[1] Y. Gao and J. Zheng, "Clearing the air through pipes? an evaluation of the air pollution reduction effect of China's natural gas pipeline projects," *Energy Policy*, vol. 160, 2022, Art. no. 112649.

[2] H. A. Kishawy and H. A. Gabbar, "Review of pipeline integrity management practices," *Int. J. Press. Vessels Piping*, vol. 87, no. 7, pp. 373–380, 2010.

[3] I. N. Ismail et al., "Development of in-pipe inspection robot: A review," in *Proc. IEEE Conf. Sustain. Utilization Develop. Eng. Technol.*, 2012, pp. 310–315.

[4] E. Dertien, S. Stramigioli, and K. Pulles, "Development of an inspection robot for small diameter gas distribution mains," in *Proc. IEEE Int. Conf. Robot. Automat.*, 2011, pp. 5044–5049.

[5] Y.-S. Kwon, B. Lee, I.-C. Whang, W.-K. Kim, and B.-J. Yi, "A flat pipeline inspection robot with two wheel chains," in *Proc. IEEE Int. Conf. Robot. Automat.*, 2011, pp. 5141–5146.

[6] M. Gao, M. Huang, K. Tang, X. Lang, and J. Gao, "Design, analysis, and control of a multilink magnetic wheeled pipeline robot," *IEEE Access*, vol. 10, pp. 67168–67180, 2022.

[7] C. Rusu and M. O. Tatar, "Adapting mechanisms for in-pipe inspection robots: A review," *Appl. Sci.*, vol. 12, no. 12, 2022, Art. no. 6191.

[8] T. Ren, Y. Zhang, Y. Li, Y. Chen, and Q. Liu, "Driving mechanisms, motion, and mechanics of screw drive in-pipe robots: A review," *Appl. Sci.*, vol. 9, no. 12, 2019, Art. no. 2514.

[9] H. Fukushima, S. Satomura, T. Kawai, M. Tanaka, T. Kamegawa, and F. Matsuno, "Modeling and control of a snake-like robot using the screw-drive mechanism," *IEEE Trans. Robot.*, vol. 28, no. 3, pp. 541–554, Jun., 2012.

[10] W. Zhao, L. Zhang, and J. Kim, "Design and analysis of independently adjustable large in-pipe robot for long-distance pipeline," *Appl. Sci.*, vol. 10, no. 10, 2020, Art. no. 3637.

[11] A. Kakogawa, S. Ma, and S. Hirose, "An in-pipe robot with underactuated parallelogram crawler modules," in *Proc. IEEE Int. Conf. Robot. Automat.*, 2014, pp. 1687–1692.

[12] K. Hoon, G. Sharma, and S. Iyengar, "FAMPER: A fully autonomous mobile robot for pipeline exploration," in *Proc. IEEE Int. Conf. Ind. Technol.*, 2010, pp. 14–17.

[13] K. Suryavanshi, R. Vadapalli, R. Vucha, A. Sarkar, and K. M. Krishna, "Omnidirectional tractable three module robot," in *Proc. IEEE Int. Conf. Robot. Automat.*, 2020, pp. 9316–9321.

[14] A. Kakogawa and S. Ma, "A multi-link in-pipe inspection robot composed of active and passive compliant joints," in *Proc. IEEE/RSJ Int. Conf. Intell. Robots Syst.*, 2020, pp. 6472–6478.

[15] J. Cao, W. Liang, Y. Wang, H. P. Lee, J. Zhu, and Q. Ren, "Control of a soft inchworm robot with environment adaptation," *IEEE Trans. Ind. Electron.*, vol. 67, no. 5, pp. 3809–3818, May 2020.

[16] M. Inazawa, T. Takemori, M. Tanaka, and F. Matsuno, "Motion design for a snake robot negotiating complicated pipe structures of a constant diameter," in *Proc. IEEE Int. Conf. Robot. Automat.*, 2020, pp. 8073–8079.

[17] F. Trebuňa, I. Virgala, M. Pástor, T. Lipták, and L. Miková, "An inspection of pipe by snake robot," *Int. J. Adv. Robot. Syst.*, vol. 13, no. 5, 2016, Art. no. 1729881416663668.

[18] K. Kotay and D. Rus, "The inchworm robot: A multi-functional system," *Auton. Robots*, vol. 8, no. 1, pp. 53–69, 2000.

[19] K. Hayashi et al., "Improvement of pipe holding mechanism and inchworm type flexible pipe inspection robot," *Int. J. Mech. Eng. Robot. Res.*, vol. 9, no. 6, pp. 894–899, 2020.

[20] Y. Lin, Y.-X. Xu, and J.-Y. Juang, "Single-actuator soft robot for in-pipe crawling," *Soft Robot.*, vol. 10, no. 1, pp. 174–186, 2023.

[21] Y. Liu et al., "A tensegrity-based inchworm-like robot for crawling in pipes with varying diameters," *IEEE Robot. Automat. Lett.*, vol. 7, no. 4, pp. 11553–11560, Oct. 2022.

[22] D. S. Shah et al., "Tensegrity robotics," *Soft Robot.*, vol. 9, no. 4, pp. 639–656, 2022.

[23] J. B. Haurum and T. B. Moeslund, "Sewer-ML: A multi-label sewer defect classification dataset and benchmark," in *Proc. IEEE/CVF Conf. Comput. Vis. Pattern Recognit.*, 2021, pp. 13456–13467.